SIAM J. APPL. MATH.
Vol. 65, No. 4, pp. 1420–1442

DIFFUSIVE AND CHEMOTACTIC CELLULAR MIGRATION: SMOOTH AND DISCONTINUOUS TRAVELING WAVE SOLUTIONS*

K. A. LANDMAN†, M. J. SIMPSON†, J. L. SLATER†, AND D. F. NEWGREEN‡

Abstract. A mathematical model describing cell migration by diffusion and chemotaxis is considered. The model is examined using phase plane, numerical, and perturbation techniques. For a proliferative cell population, traveling wave solutions are observed regardless of whether the migration is driven by diffusion, chemotaxis, or a combination of the two mechanisms. For pure chemotactic migration, both smooth and discontinuous solutions with shocks are shown to exist using phase plane analysis involving a curve of singularities, and identical results are obtained numerically. Alternatively, pure diffusive migration and combinations of diffusive and chemotactic migration yield smooth solutions only. For all cases the wave speed depends on the exponential decay rate of the initial cell density, and it is bounded by a minimum value which is numerically observed whenever the initial cell distribution has compact support. The minimum wave speed c_{min} is proportional to $\sqrt{\chi}$ or $\sqrt{D}$ for pure chemotaxis and pure diffusion cases, respectively. The value of c_{min} for combined diffusion and chemotactic migration is examined numerically. The rate at which the mixed migration system approaches either a diffusion-dominated or chemotaxis-dominated system is investigated as a function of a dimensionless parameter involving D/χ. Finally, a perturbation analysis provides details of the steep critical layer when $D/\chi \ll 1$, and these are confirmed with numerical solutions. This analysis provides a deeper qualitative and quantitative understanding of the interplay between diffusion and chemotaxis for invading cell populations.

Key words. migration, chemotaxis, diffusion, traveling wave, numerical solution, phase plane, shock, wave speed

AMS subject classifications. 34A34, 35L40, 35L67, 92C17, 35K57, 92C15, 65M99

DOI. 10.1137/040604066

1. Introduction.

Cell migration is an essential feature of many important biological systems, including wound healing, tumor invasion, and several developmental biology processes [12, 27, 37]. Typically, to model cell migration, a system of conservation equations is proposed which incorporates the migratory processes in conjunction with kinetic terms to simulate proliferation of the migratory population. Additional kinetic processes (e.g., cell death, cell-receptor binding) can be included in the kinetic terms where required. Diffusion and chemotaxis are two common cell migration mechanisms [5].

Diffusion simulates random walk processes of cells. The Fisher equation [6] is the archetypal pure diffusion model which considers diffusive migration together with proliferation of cells via a logistic process.

Chemotaxis describes the movement of cells in the direction of a spatial gradient of a signaling species called the chemoattractant. The chemoattractant kinetics may be specified in several ways. An early chemotactic model was developed by Keller and Segel [13] describing bacterial motion. Other important contributions have been

*Received by the editors February 10, 2004; accepted for publication (in revised form) October 12, 2004; published electronically April 26, 2005. This research was supported by National Health and Medical Research Council project grant ID237144.

http://www.siam.org/journals/siap/65-4/60406.html

†Department of Mathematics and Statistics, University of Melbourne, Victoria 3010, Australia (k.landman@ms.unimelb.edu.au, m.simpson@ms.unimelb.edu.au, j.slater@ms.unimelb.edu.au). The research of the first author was supported by the Particulate Fluids Processing Center, an Australian Research Council ARC Special Research Center.

‡Embryology Laboratory, Murdoch Childrens Research Institute, Royal Children's Hospital, Parkville, Victoria 3052, Australia (don.newgreen@mcri.edu.au).

made by Tranquillo [39], Tranquillo and Alt [40], Hillen [10], Othmer and Stevens [29], and Horstmann and Stevens [11], as well as those reviewed by Ford and Cummings [7].

The classical Fisher model and several pure chemotaxis models [1, 18, 24, 25, 31, 32] are known to support traveling wave solutions moving with a constant speed. For the Fisher model, the wave speed is bounded by a minimum value [25]. For pure chemotactic migration, Landman, Pettet, and Newgreen [18] recently demonstrated the existence of traveling wave solutions with a minimum wave speed. It should be noted that haptotaxis, which is based on migration along adhesive extracellular matrix gradients, is mathematically equivalent to chemotaxis; hence a pure haptotactic model can also support traveling wave solutions with a minimum wave speed [20, 22, 30]. The focus of these previous analyses has been to examine the characteristics of traveling wave solutions for cell migration in response to a single mechanism. The more complex case of multimechanism migration has received less attention and is therefore poorly understood.

In this article we consider a model of diffusive and chemotactic cell migration. The model is motivated by migration processes during embryological development. The rostral-to-caudal migration of neural crest cells along the developing avian and mammalian intestine is one of the most extensive migration paths known in developmental biology [15]. Neural crest cells show a variety of responses including chemotactic attraction to growth factors, which are thought to be produced uniformly along the intestine mesenchymal tissue (e.g., glial derived neurotrophic factor (GDNF) [43]). Local gradients in the chemoattractant concentration are postulated to arise from the binding of the chemoattractant to receptors on the migrating cells, rather than from diffusion of growth factors from a source. In addition to promoting migration, the chemoattractant also acts as a survival factor for the migrating population [9, 26, 43]. Interest in the migration of enteric neural crest cells stems from hypotheses which have linked neural crest cell migration to a common birth defect in humans called Hirschsprung's disease or aganglionic megacolon. This defect occurs when the caudal part of the gut lacks intrinsic nerve cells. Hirschsprung's disease is thought to occur when the rostral-to-caudal migration of the neural crest cells fails to completely colonize the developing intestine [17, 28].

This paper constructs a mathematical framework for the analysis of the combined diffusive and chemotactic migration, relevant to developmental biology processes. We utilize a holistic approach incorporating both analytical and numerical analyses of traveling wave solutions for the proposed model. For the case of purely chemotactic migration, the results presented here extend the previous work of Landman, Pettet, and Newgreen [18] in two significant ways. First, the relationship between the wave speed and the transition from smooth to discontinuous solutions is examined in detail. Second, an analysis of the functional dependence of the minimum wave speed for pure chemotaxis migration is presented. This analysis provides a useful relationship similar to the well-known expression for the Fisher equation.

For the more complex case of combined diffusion and chemotaxis migration we use a specifically designed numerical algorithm to examine the traveling wave solutions. In particular, the numerical results are used to show how the combined diffusive and chemotactic migration model approaches the limits of diffusion-only and chemotaxis-only cases as the relative contributions of diffusion and chemotaxis are altered. This kind of analysis is unexplored in previous studies [18, 21]. We use the numerically determined wave speeds to conjecture some useful bounds on the minimum wave speed

for the combined diffusion and chemotaxis problem.

The mathematical model for this problem is a coupled system of partial differential equations for cell density and chemoattractant concentration. A traveling wave coordinate system is introduced with an unknown wave speed to convert the system into a coupled system of ordinary differential equations. Phase plane and singular perturbation methods are then used to explore the solutions of the system. The numerical algorithm is applicable to pure hyperbolic problems including the formation of shock-fronted solutions as well as parabolic problems.

2. Diffusive and chemotactic cell migration in one dimension. A system of equations is introduced to describe the diffusive and chemotactic migration of cells in one dimension. Let $n(x,t)$ and $g(x,t)$ denote the cell density and chemoattractant concentration per unit length, respectively; x and t are position and time coordinates. A conservation-of-mass argument for a diffusion and chemotaxis transport of cells gives

$$\frac{\partial n}{\partial t} = D\frac{\partial^2 n}{\partial x^2} - \chi\frac{\partial}{\partial x}\left(n\frac{\partial g}{\partial x}\right) + f(n,g), \tag{2.1}$$

$$\frac{\partial g}{\partial t} = h(n,g), \tag{2.2}$$

where the diffusion coefficient D and the chemotactic factor χ are assumed to be constant [20, 21, 22]. The assumption of a constant chemotactic factor ignores saturation effects. Although alternative forms for $\chi(g)$ that incorporate saturation have been proposed [8], the specific relationship relevant to the system of interest is unknown and therefore a constant value is adopted. Preliminary investigations indicate that the results of this study are qualitatively insensitive to this assumption. The f and h terms in (2.1)–(2.2) represent the kinetic terms. Equation (2.2) reflects our assumption that the distribution of chemoattractant is governed by kinetic processes rather than diffusion. This is particularly relevant for the migration of neural crest cells where the chemoattractant GDNF is produced uniformly within the underlying tissues and not from diffusion from some external source [43]. For this case, the distribution of chemoattractant is governed by a balance between the underlying production of chemoattractant, the natural decay of chemoattractant, and also the uptake of chemoattractant by the migrating cells. Furthermore, care must be taken to ensure that the steady state of (2.2) does not permit a zero solution as the chemoattractant is a trophic factor necessary for the survival of the migratory population. Therefore, the chemoattractant concentration must be strictly positive at all times to sustain the migratory species.

In keeping with these biologically motivated considerations, the kinetic terms are chosen to reflect the following assumptions. The cells n proliferate by mitosis and have a carrying capacity density; these characteristics can be described by a logistic-type term for f. The chemoattractant g is produced uniformly at a constant rate throughout the domain and decays with time. Furthermore, the chemoattractant binds to the cells. Therefore a localized initial distribution of cells creates a gradient of chemoattractant, which produces a chemoattractant migration velocity. These effects are described with the following choice of f and h:

$$f = \lambda_1 n\left(1 - \frac{n}{k_1}\right), \tag{2.3}$$

$$h = \lambda_2 - \lambda_3 g - \lambda_4 n g. \tag{2.4}$$

For simplicity, a constant mitotic index λ_1 is assumed rather than a more complex form with $\lambda_1(g)$.

The system (2.1)–(2.4) reduces to some special cases. When the chemotactic factor χ is zero, the equation describing the cell population n reduces to the Fisher equation [6, 25]. Alternatively, when the diffusivity D is zero, cell migration is driven by chemotaxis alone. Several authors (e.g., [2, 18, 32]) have studied some aspects of simple chemotaxis models, or mathematically equivalent haptotaxis models, with a different choice of kinetic term h. The choice of h here is governed by considerations relevant to developmental biology problems as discussed.

We are interested in cells at their maximum density migrating into a region without such cells, giving rise to an invading profile with a constant shape and moving at a constant speed. The well-studied Fisher equation allows such traveling wave solutions, while purely chemotactic systems also support such solutions [18]. The nature of such solutions, whether they are smooth or discontinuous functions, and their minimum wave speed will be investigated here.

Scaling time with the mitotic index and introducing a length scale L, all the variables can be made dimensionless using the definitions as shown:

$$n = k_1 n^*, \qquad g = \frac{\lambda_2}{\lambda_3} g^*, \qquad t = \frac{1}{\lambda_1} t^*, \qquad x = L x^*, \tag{2.5}$$

$$D^* = \frac{D}{L^2 \lambda_1}, \qquad \chi^* = \frac{\chi \lambda_2}{L^2 \lambda_1 \lambda_3}, \qquad \beta = \frac{\lambda_3}{\lambda_1}, \qquad \gamma = \frac{\lambda_4 k_1}{\lambda_1}. \tag{2.6}$$

In later sections we choose L so that one of the dimensionless parameters D^* or χ^* is equal to unity. Omitting the asterisk notation, the dimensionless system is

$$\frac{\partial n}{\partial t} = D \frac{\partial^2 n}{\partial x^2} - \chi \frac{\partial}{\partial x}\left(n \frac{\partial g}{\partial x} \right) + n(1-n), \tag{2.7}$$

$$\frac{\partial g}{\partial t} = \beta(1-g) - \gamma n g. \tag{2.8}$$

To explore the nature of the dynamics of the system (2.7)–(2.8), we consider numerical solutions in conjunction with phase plane and perturbation analyses.

3. Numerical solution. Numerical solutions to the full system (2.7)–(2.8) are sought. We are interested in obtaining results under a wide range of conditions where diffusion or chemotaxis can either dominate or be absent. Therefore, the numerical scheme must be sufficiently robust to solve either a purely hyperbolic system ($D = 0$) or the simpler diffusion-reaction system ($\chi = 0$). An operator splitting technique is used to overcome this difficulty [16, 38, 36, 41]. Within each time increment, temporal integration of the system (2.7)–(2.8) is split into two steps. First the purely hyperbolic system (2.7)–(2.8) with $D = 0$, namely,

$$\frac{\partial n}{\partial t} = -\chi \frac{\partial}{\partial x}\left(n \frac{\partial g}{\partial x} \right) + n(1-n), \tag{3.1}$$

$$\frac{\partial g}{\partial t} = \beta(1-g) - \gamma n g, \tag{3.2}$$

is solved to yield intermediate solutions. Second, these intermediate solutions are used as initial conditions to solve the remaining parabolic system

$$\frac{\partial n}{\partial t} = D \frac{\partial^2 n}{\partial x^2}, \tag{3.3}$$

$$\frac{\partial g}{\partial t} = 0. \tag{3.4}$$

Obtaining numerical solutions of linear hyperbolic problems using standard numerical schemes has been referred to as an "embarrassingly difficult problem" [42]. Therefore, the greatest of care must be exercised in obtaining numerical solutions of the nonlinear hyperbolic system (3.1)–(3.2). To this end, we spatially discretize (3.1)–(3.2) with the semidiscrete scheme described by Kurganov and Tadmor [14]. The resulting system of ordinary differential equations is explicitly integrated with a fourth-order Runge–Kutta algorithm using a constant time step [33]. The solution to the parabolic system (3.3)–(3.4) is obtained using a linear finite element mesh composed of uniformly spaced elements. Temporal integration of the discretized finite element equations is achieved with a mass-lumped backward Euler scheme [34]. Both spatial and temporal discretizations are uniform. We choose to include the kinetic terms in the hyperbolic step of the splitting scheme since this step is solved using an explicit method convenient for solving nonlinear kinetic terms; alternatively, if the kinetic terms are included in the parabolic step, then the implicit Euler stepping would require further iterations to solve the resulting nonlinear system of equations. From this point of view the splitting regime (3.1)–(3.4) is computationally efficient.

It should be noted that the main limitation with this numerical scheme is imposed through the hyperbolic solution method [14] which requires sufficiently small time steps so that the Courant condition is satisfied,

$$Cr = \max \frac{\mid \lambda_i \mid \Delta t}{\Delta x} \leq M, \tag{3.5}$$

where the λ_i are the eigenvalues associated with the Jacobian of the flux vector [14] and M is some constant. The λ_i relate to the speed of propagation of information for the system. Fortunately, since we are interested in traveling wave solutions which move with a constant wave speed, it is clear that a uniformly optimal time step Δt exists for a particular uniform spatial mesh. The optimal time step can be determined using a straightforward trial-and-error approach. The finite element solution of the parabolic system (3.3)–(3.4) is not subject to any numerical stability limitation since the mass-lumped implicit Euler scheme is known to be unconditionally stable [34].

The numerical scheme outlined here is particularly convenient for analyzing general solutions of the system (2.7)–(2.8). The inclusion of Kurganov and Tadmor's central scheme is necessary so that the nonlinear hyperbolic term associated with chemotactic migration can be solved accurately without incurring any high Peclet number-induced oscillations and numerical diffusion associated with standard numerical techniques [44]. Furthermore, incorporating diffusion through an operator splitting scheme is required to maintain generality of the algorithm. Previous attempts at simulating a combined haptotactic and diffusive migration system discretized the diffusion term explicitly within the central scheme [21]. This previous approach is very restrictive as explicit solutions of the diffusion equation are subject to well-known stability criteria [4] which are satisfied only for small values of the diffusion coefficient. These limitations are completely overcome in this work as the diffusion term is split and solved implicitly thereby yielding an algorithm valid for any value of χ and D.

The problem is modeled on the infinite x domain. However, for numerical computations the finite domain $[0, X]$ is selected with X chosen to be sufficiently large to avoid boundary effects. Zero-flux conditions are specified for both boundaries. Since we are interested in the invasion of cells into the domain, the initial data are chosen to be primarily localized near the left boundary as discussed in section 4.

After a particular time, the numerical solution converges to a fixed profile moving with a constant speed. The traveling wave speed c is computed by selecting a particular contour, say, $n(x,t) = N$, and locating the position of that contour at each time interval using a linear interpolation scheme. Once the position of the contour is known over successive time intervals, the wave speed can be approximated by

$$c_n = \frac{x^{n+1} - x^n}{\Delta t} \tag{3.6}$$

for large n, where x^n and x^{n+1} are the positions of the contour at the n and $n+1$ time step, respectively, and Δt is the time step. The speed of convergence varies with initial conditions and parameter values. Consequently, the domain length X must be chosen sufficiently large if the convergence is slow. When $D = 0$, the chemotactic migration cell profile is expected to develop a shock in the low-concentration region of the profile for some choices of initial condition [22]. It is impractical to use linear interpolation to determine the position of the contour within the shock because of the discontinuity. This complication is circumvented by choosing a concentration away from the shock region to compute the wave speed. Therefore, it is best to use a sufficiently large contour value N.

4. Traveling wave speed and dependence on the initial conditions. Traveling wave solutions with a range of possible wave speeds greater than some minimum value are known to occur for purely diffusive or purely chemotactic migration [6, 25, 18]. We expect the same behavior when both diffusion and chemotaxis are present. Here we investigate how various types of initial data evolve to traveling wave solutions with different wave speeds. To determine the minimum wave speed numerically, it is necessary to know the relationship between the initial conditions and the wave speed so that the appropriate initial conditions are specified.

It is possible to investigate the speed of the traveling waves by examining the leading edge of the wave, assuming it decays exponentially in space [25]. McKean [23] and Marchant [19] determine relationships between exponential decay rates of initial data and the wave speed of solutions for the Fisher equation (purely parabolic) and a haptotactic invasion (purely hyperbolic) system, respectively. We extend this work to our system with both diffusion and chemotaxis.

Consider initial conditions, where for large x

$$n(x,0) = A_1 e^{-\xi_1 x}, \tag{4.1}$$

$$g(x,0) = 1 - A_2 e^{-\xi_2 x} \tag{4.2}$$

for arbitrary positive constant A_1, A_2, ξ_1 and ξ_2. Looking at the evolving wave near the leading edge and writing $n = \tilde{n}, g = 1 - \tilde{g}$, assuming that $\tilde{n}$ and $\tilde{g}$ are small, the system (2.7)–(2.8) simplifies to the linear system

$$\frac{\partial \tilde{n}}{\partial t} = D\frac{\partial^2 \tilde{n}}{\partial x^2} + \tilde{n}, \tag{4.3}$$

$$-\frac{\partial \tilde{g}}{\partial t} = \beta \tilde{g} - \gamma \tilde{n} \tag{4.4}$$

with the initial conditions (for large x)

$$\tilde{n}(x,0) = A_1 e^{-\xi_1 x}, \tag{4.5}$$

$$\tilde{g}(x,0) = A_2 e^{-\xi_2 x}. \tag{4.6}$$

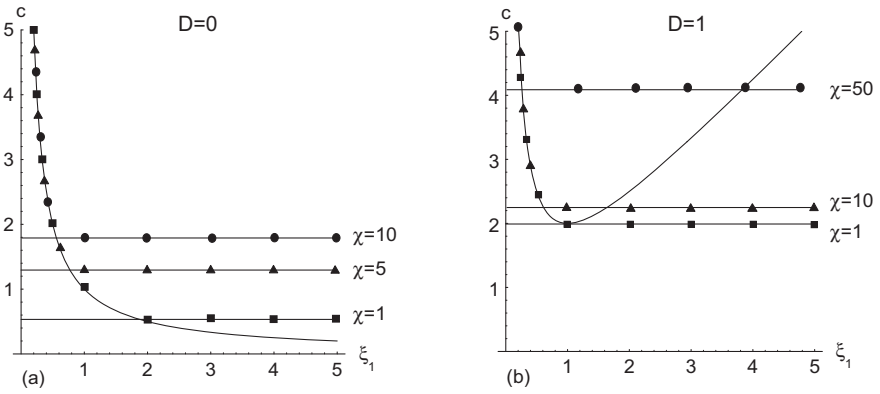

FIG. 4.1. *Numerical wave speed c versus ξ_1 for initial data of the form* (4.1)–(4.2). *Numerical results are shown in squares, circles, and triangles. These results were generated using* $\Delta x = 0.05$ *and* $\Delta t = 0.01$. *The continuous curves are given by* (4.7). *The horizontal lines represent* c_{min}. *Here* $\beta = 1$ *and* $\gamma = 1$. (*a*) *With* $D = 0$ *and increasing values of* χ. (*b*) *With* $D = 1$ *and increasing values of* χ.

A solution of the form $\tilde{n} = A_1 e^{-\xi_1(x-ct)}$ is sought. Substitution into (4.3)–(4.4) requires

$$c = \frac{1}{\xi_1} + D\xi_1 \tag{4.7}$$

for large values of x. Then solving (4.4) with (4.6), the leading edge of chemoattractant concentration is

$$\tilde{g} = e^{-\beta t}\left[A_2 e^{-\xi_2 x} - \frac{\gamma A_1}{\beta + \xi_1 c} e^{-\xi_1 x}\right] + \frac{\gamma A_1}{\beta + \xi_1 c} e^{-\xi_1(x-ct)}. \tag{4.8}$$

For large values of t, both $\tilde{n}$ and $\tilde{g}$ are functions of the traveling wave coordinate $x - ct$, where c is given by (4.7). This condition is independent of ξ_2 and hence independent of the initial conditions imposed on g.

The analytical result for c given by (4.7) is confirmed by the numerical results illustrated in Figure 4.1. Two cases are described. In the first, $D = 0$, so that the cells are purely chemotactically driven. For fixed values of the kinetic parameters β and γ and chemotactic factor χ, Figure 4.1(a) shows that a traveling wave solution with wave speed satisfying (4.7) is realized when $\xi_1 < 1/c_{min}$. Alternatively, when $\xi_1 > 1/c_{min}$ a traveling wave of fixed wave speed develops where $c = c_{min}$. Furthermore Figure 4.1(a) shows that c_{min} increases proportional to $\sqrt{\chi}$. In section 6.2, both smooth and discontinuous solutions will be found numerically using initial data of the form (4.1)–(4.2) (with $\xi_2 = 0$). (Note that (4.7) is also valid when both $D = \chi = 0$; under these conditions a traveling wave results from the initial nonzero cell density distribution in conjunction with the kinetics.) The second case, $D = 1$, $\chi > 0$, illustrated in Figure 4.1(b), has the same qualitative behavior as the case $D = 0$. The solution with $\chi = 0$ corresponds to the Fisher equation ($c_{min} = 2$, [25]) and is not shown here. As χ increases the value of c_{min} again increases, but for the case of nonzero D, it clearly does not scale with $\sqrt{\chi}$.

In summary, numerical computations yield a suite of traveling waves with the wave speed dependent on the exponential decay rate of the initial cell population

$n(x,0)$. There is a maximum exponential decay rate such that for ξ_1 larger than the maximum value, the initial data develops into a traveling wave moving with a minimum wave speed c_{min}. Further discussion of c_{min} will appear in section 6.3.2.

The asymptotic form of the initial conditions given by (4.1)–(4.2) is useful for numerically investigating the dependence of the wave speed on the decay rate ξ_1. However, in the limit $\xi_1 \to \infty$ the initial cell distribution tends towards having semi-compact support, a typical choice being

$$n(x,0) = \begin{cases} 1, & x < x_1, \\ q(x), & x_1 < x < x_2, \\ 0, & x > x_2, \end{cases} \tag{4.9}$$

where $q(x)$ is monotonic and continuous. Since all such functions decay faster than any exponential function, $n(x,t)$ will evolve to a traveling wave with speed $c = c_{min}$. Numerical solutions with such initial data confirm this result.

In light of this discussion, initial conditions used in this study take the form

$$n(x,0) = \begin{cases} 1, & x < 10, \\ e^{-\xi_1(x-10)}, & x \geq 10, \end{cases} \tag{4.10}$$

$$g(x,0) \equiv 1. \tag{4.11}$$

Altering the value of ξ_1 in (4.10) enables the leading front of the cell density distribution to decay exponentially with a variable rate. In the limit $\xi_1 \to \infty$ the initial conditions (4.10) approach a step function at $x = 10$. This is a particular case of the more general initial condition (4.9) with $x_1 = x_2 = 10$. The location of the transition point to exponential decay is arbitrary as identical traveling wave behavior results regardless of the point chosen.

5. Traveling wave solution. Introducing the traveling wave coordinate transformation $z = x - ct$, where c is the dimensionless wave speed, and the variable $v = \frac{\partial n}{\partial x}$, the dimensionless system (2.7)–(2.8) becomes the following first-order system of equations:

$$c\frac{dg}{dz} = -\left[\beta(1-g) - \gamma n g\right], \tag{5.1}$$

$$\frac{dn}{dz} = v, \tag{5.2}$$

$$\begin{aligned} D\frac{dv}{dz} = {} & \frac{\chi n}{c^2}\left[\gamma n + \beta\right]\left[\gamma n g - \beta(1-g)\right] - n(1-n) \\ & - \left[1 + \frac{\chi}{c^2}(\beta(1-g) - 2\gamma n g)\right] cv. \end{aligned} \tag{5.3}$$

There are two steady states of this system, namely, $(g,n,v) = (\frac{\beta}{\beta+\gamma}, 1, 0)$ and $(1,0,0)$. The first state corresponds to cells at their carrying capacity density and therefore can be thought of as the colonized or invaded state, whereas the second is the uncolonized state. We seek traveling wave solutions connecting the colonized to the uncolonized state. Note that $\frac{\beta}{\beta+\gamma}$ is a function which depends only on the ratio γ/β; it is an increasing function of the production rate β, is a decreasing function of binding rate γ, and is always less than unity, the value of the chemoattractant concentration in the absence of cells.

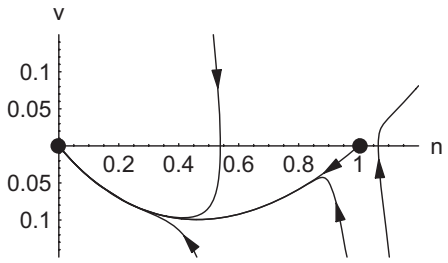

FIG. 6.1. *Phase plane for the Fisher equation. Here* $D = 1$, $c = 2.5$. *The steady states are marked* (•).

6. Phase plane, perturbation analysis, and numerical solutions. We first investigate phase plane and numerical solutions corresponding to the two special cases when one of D or χ is zero and discuss the nature of the solutions and the minimum wave speed c_{min}. For the remaining case, when both migration mechanisms are active, the transition from Fisher type solutions to chemotactic solutions (and vice versa) is investigated, and the solutions and c_{min} are determined numerically. In addition, perturbation analysis provides some insight into any rapid transition zones.

6.1. Diffusion-driven migration, no chemotaxis. If the chemotactic coefficient is zero, then the model equations reduce to the Fisher equation which describes cell migration driven by diffusion and proliferation. Then the system (2.7)–(2.8), in the traveling wave coordinate, reduces to the differential equation system

$$\frac{dn}{dz} = v, \tag{6.1}$$

$$D\frac{dv}{dz} = -n(1-n) - cv. \tag{6.2}$$

It is well known that traveling waves exist and can be found by phase plane analysis in the (n, v) plane, as illustrated in Figure 6.1. The state $(n, v) = (1, 0)$ is a saddle for all values of c. The other steady state (0,0) is a stable node if $c^2 > 4D$ and a stable spiral if $c^2 < 4D$. The population density n is required to be nonnegative and hence cannot be oscillatory around zero; therefore, the wave speed must be restricted to $c^2 \geq 4D$ giving a minimum wave speed $c_{min} = 2\sqrt{D}$. The traveling wave solutions are smooth. Clearly, the cell density is independent of the chemoattractant kinetics.

Numerical solutions to (2.7)–(2.8) with $\chi = 0$ are shown in Figure 6.2 with both rapid and slowly decaying initial conditions. In both cases, the profiles of $n(x, t)$ show clear traveling wave behavior characterized by a constant wave speed. For rapidly decaying initial conditions, Figure 6.2(a) demonstrates a minimum wave speed of $c_{min} = 2.0$, which agrees with the theoretical result. Alternatively for slowly decaying initial conditions, Figure 6.2(b) illustrates an increased wave speed of $c = 2.5$, as given by (4.7). This example confirms the result that the traveling wave speed c depends on the exponential decay rate of the initial distribution of the cell population.

6.2. Chemotactically driven migration, no diffusion. If the diffusion coefficient is zero, then the variable v does not need to be introduced. As discussed in section 2, when there is no diffusion, we can choose the length scale L so that the dimensionless χ is identically equal to unity. Then equations (5.1)–(5.3) reduce to the

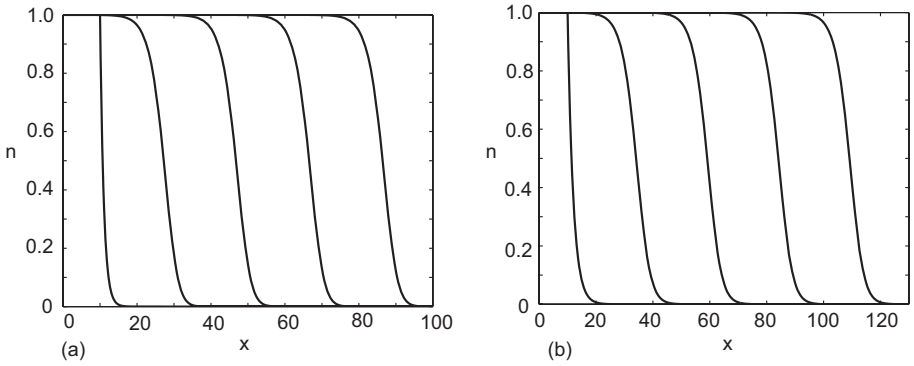

FIG. 6.2. *Numerical solutions of $n(x,t)$ for the Fisher equation with $D = 1$, $\Delta x = 0.05$, and $\Delta t = 0.01$. (a) Solutions at $t = 0, 10, 20, 30$, and 40 left to right with $\xi_1 = 10$. The computed wave speed is $c = c_{min} = 2$. (b) Solutions at $t = 0, 10, 20, 30$, and 40 left to right with $\xi_1 = 0.5$. The computed wave speed is $c = 2.5$.*

following system:

$$c\frac{dg}{dz} = -\left[\beta(1-g) - \gamma n g\right], \tag{6.3}$$

$$c\left[1 + \frac{1}{c^2}(\beta(1-g) - 2\gamma n g)\right]\frac{dn}{dz} = \frac{n}{c^2}\left[\gamma n + \beta\right]\left[\gamma n g - \beta(1-g)\right] - n(1-n). \tag{6.4}$$

The chemoattractant kinetic term h chosen here differs from that in [18], resulting in a different system with different steady states. The steady states of (6.3)–(6.4) are $(g,n) = (\frac{\beta}{\beta+\gamma}, 1)$ and (1,0). The point $(\frac{\beta}{\beta+\gamma}, 1)$ is an unstable focus when $c^2 > \frac{\beta\gamma}{\beta+\gamma}$ and is a saddle when $c^2 < \frac{\beta\gamma}{\beta+\gamma}$, while the point (1,0) is always a saddle. It is worth noting that with no diffusion, the stability of the steady states does not provide a minimum for the wave speed, since the eigenvalues are always real.

When the function premultiplying $\frac{dn}{dz}$ in (6.4) is identically zero, the derivative $\frac{dn}{dz}$ is no longer defined. Pettet, McElwain, and Norbury [32] defined such a curve as a *wall-of-singularities*. Here the wall-of-singularities can be written as

$$n = \frac{1}{2\gamma g}\left(c^2 + \beta(1-g)\right). \tag{6.5}$$

This wall is asymptotic to the n-axis, cutting the positive g-axis at

$$g = 1 + \frac{c^2}{\beta}$$

to the right of the steady state $(1,0)$. Hence when $c^2 > \frac{\beta\gamma}{\beta+\gamma}$ the two steady states (an unstable focus and a saddle) are to the left of the wall. Alternatively, when $c^2 < \frac{\beta\gamma}{\beta+\gamma}$, then the two steady states (both saddles) are on either side of the wall. The wall gets closer to the origin as c^2 decreases, and therefore it is possible for the wall to move below the steady state $(\frac{\beta}{\beta+\gamma}, 1)$.

Pettet, McElwain, and Norbury [32] showed that a solution approaching a wall-of-singularities could not cross the wall unless it passed through a special point called a *hole* in the wall. A hole is defined by both the function premultiplying $\frac{dn}{dz}$ and the

right-hand side of (6.4) being equal to zero simultaneously. Marchant, Norbury, and Perumpanani [20] and Landman, Pettet, and Newgreen [18] showed that for a system of equations (in the class of (2.1)–(2.2)) a trajectory exiting one steady state in the phase plane which passed through a hole in the wall could in fact recross the wall by way of a jump discontinuity to join up with the second steady state.

Similar behavior, where the two steady states are on same side of the wall, occurs for the system considered here. As noted, our system also allows the two steady states to be on the opposite sides of the wall. We will show that for this case the presence of a hole in the wall is irrelevant and all traveling wave solutions exhibit a shock or discontinuity. For this problem, there is at most one hole in the wall in the positive (g, n) quadrant.

In seeking a trajectory connecting $(\frac{\beta}{\beta+\gamma}, 1)$ to $(1, 0)$, two different types of behavior can occur, and these are explained with two examples.

Example 1. In our first example, Figure 6.3 illustrates the (g, n) phase plane with decreasing values of wave speed c, for one choice of the kinetic parameters β and γ. For sufficiently large wave speeds, the two steady states are below the wall as in Figure 6.3(a) and there is a unique trajectory to the left of the wall, connecting the two states; this gives a smooth traveling wave. However, as c is decreased, there is a value $c = c_{crit}$ where the wall begins to interfere with trajectories emanating from the unstable node. At this value the trajectory just touches the hole in the wall as in Figure 6.3(b). For $c < c_{crit}$, we must determine whether a trajectory emanating from $(\frac{\beta}{\beta+\gamma}, 1)$ can cross the wall and connect to the other steady state (1,0).

Marchant [19] and Landman, Pettet, and Newgreen [18] investigated a similar scenario. The arguments in section 4 of [18] for general kinetic terms apply to our system of equations, allowing us to summarize the results here. No smooth connection between the two states can be made; however, there is the possibility for the solution to be nonsmooth by containing a jump discontinuity. The method relies on hyperbolic partial differential equation theory, Lax entropy condition, and the Rankine–Hugoniot jump condition. A solution for n with a shock or discontinuity, traveling of course with the constant wave speed c, is shown to exist. Let the subscripts L and R denote the value of the variable on the left and right side of the shock, respectively. Then from (4.10)–(4.12) in [18], with $h = \beta(1 - g) - \gamma n g$, the shock conditions are

$$g_L = g_R = g, \tag{6.6}$$

$$n_L + n_R = \frac{1}{\gamma g}\left(c^2 + \beta(1 - g)\right), \tag{6.7}$$

$$u_L - u_R = \frac{\gamma g}{c}(n_L - n_R), \tag{6.8}$$

where $u = \frac{\partial g}{\partial x}$. These equations establish that g is continuous, while n and the spatial gradient of the chemoattractant concentration u support a discontinuity. The Lax entropy condition [3] is satisfied only if $n_L > n_R$. Recall that the wall-of-singularities satisfies (6.5). Hence, from (6.7) the geometric center of the jump $\frac{1}{2}(n_L + n_R)$ lies exactly on the wall-of-singularities, and therefore any jump takes the trajectory to the other side of the wall. In this way, it is possible for a trajectory to pass through the hole in the wall and then jump to a trajectory on the other side of the wall, thus connecting the colonized and uncolonized states when $c < c_{crit}$, although the wall prevents a smooth joining trajectory. Such a case is shown in Figure 6.3(c), where the discontinuity corresponds to the vertical portion of the trajectory that joins the colonized and uncolonized steady states. After the jump discontinuity, n will have a

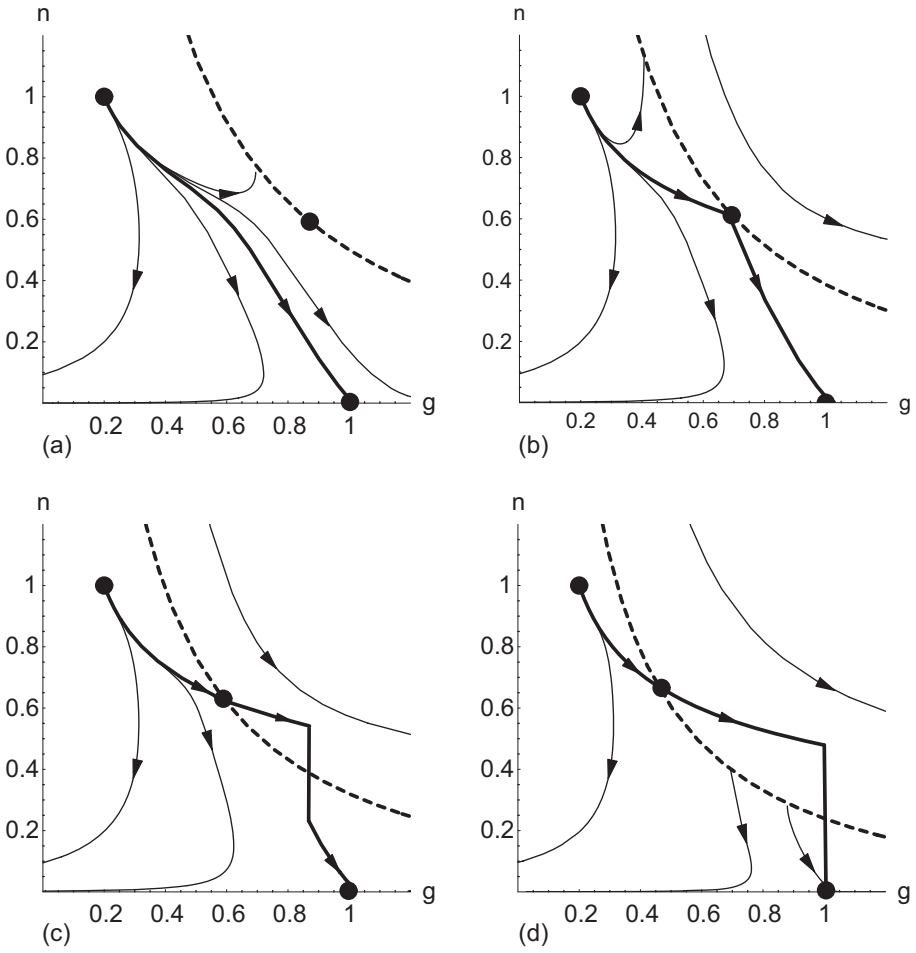

FIG. 6.3. *Phase plane for* (g, n) *for decreasing values of wave speed* c. *Here* $\beta = 0.25$, $\gamma = 1.0$. *The positions of the steady states* (•), *wall-of-singularities* (*dotted line*), *holes in the wall* (•), *and the trajectory joining the colonized and uncolonized steady states* (*thick line*) *are shown. The vertical lines in* (c) *and* (d) *correspond to the jump discontinuity in* n. (a) $c = 1.0$, (b) $c = c_{crit} \approx 0.88$, (c) $c = 0.8$, (d) $c = c_{min} \approx 0.69$.

smooth leading edge which asymptotes to zero.

However, for a realistic solution, $n_R > 0$, so the jump cannot be so large as to take the trajectory across the g-axis. As c decreases, the jump size becomes larger, until at some $c = c_{min}$, the trajectory jumps directly from $(g, n) = (1, c^2/\gamma)$ to $(1, 0)$, as illustrated in Figure 6.3(d). This solution with $c = c_{min}$ is the only solution with a zero leading edge and hence has compact support. If $c < c_{min}$, no smooth or nonsmooth traveling shock wave solution exists.

Therefore, our system supports traveling shock wave solutions with wave speed $c_{crit} > c > c_{min}$. Clearly for this example $c_{min}^2 > \frac{\beta\gamma}{\beta+\gamma}$, since both steady states remain on the same side of the wall. Example 2 considers the alternative case.

Example 2. In our second example, the value of the production rate β is increased sufficiently, so that $c_{min}^2 < \frac{\beta\gamma}{\beta+\gamma}$, allowing the possibility for the two steady states to lie on opposite sides of the wall, as shown in Figure 6.4. For sufficiently large wave

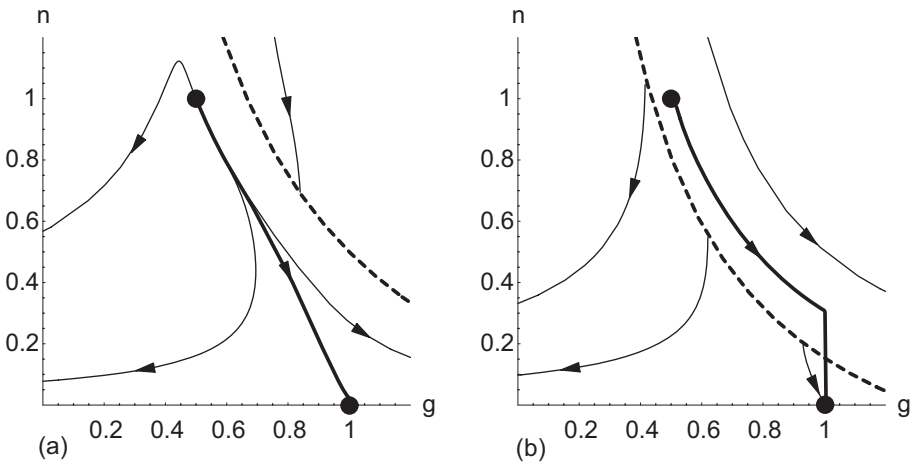

FIG. 6.4. *Phase plane for* (g, n) *for decreasing values of wave speed* c. *Here* $\beta = 1.0$, $\gamma = 1.0$. *The positions of the steady states* (•), *wall-of-singularities* (*dotted line*), *and the trajectory joining the colonized and uncolonized steady states* (*thick line*) *are shown. The vertical line in* (b) *corresponds to the jump discontinuity in* n. (a) $c = 1.0$, (b) $c = c_{min} \approx 0.556$.

speeds, the two steady states are below the wall, as in Figure 6.4(a), and there is a unique trajectory to the left of the wall, connecting the two states; this gives a smooth traveling wave. However, as c is decreased to c_{crit} where

$$c_{crit}^2 = \frac{\beta\gamma}{\beta + \gamma}, \tag{6.9}$$

the steady state lies on the wall and so is also a hole in the wall. For $c < c_{crit}$, the steady state lies on the other side of the wall, as shown in Figure 6.4(b). The jump discontinuity theory can then be applied again, so that the trajectory emanating from $(\frac{\beta}{\beta+\gamma}, 1)$ can cross the wall to join with a trajectory which connects with the saddle at (1,0). Again, the requirement that $n_R > 0$ implies that as c decreases, the jump size becomes larger, until at some $c = c_{min}$, the trajectory jumps directly from $(g, n) = (1, c^2/\gamma)$ to $(1, 0)$. If $c < c_{min}$, no smooth or nonsmooth traveling shock wave solution exists. Note that, for this case, no hole is needed when the two steady states are on opposite sides of the wall, as shown here.

In addition to the phase plane analysis, a numerical solution to the system (2.7)–(2.8) with $D = 0$ illustrates the smooth and discontinuous solutions and their corresponding dependence on the wave speed. As discussed in section 4 the wave speed depends on the exponential decay rate of the initial data for n, and therefore the mechanism for generating the smooth and discontinuous traveling waves is through varying the rate of decay ξ_1.

With the same parameter values as in Figure 6.4, profiles of n and g at a fixed time for three cases where the initial cell density distribution decreases at a rapid, moderate, and slow exponential rate are given in Figure 6.5. The left-most profile corresponds to a rapidly decaying initial condition. The cell density profile shows that the cell front is discontinuous, with the discontinuity extending to $n = 0$, and therefore the profile has compact support. The gradient of the chemoattractant profile is also discontinuous at the same position, namely, the smallest value of x where $g = 1$. This corresponds to the case where the trajectory in the phase plane jumps across the

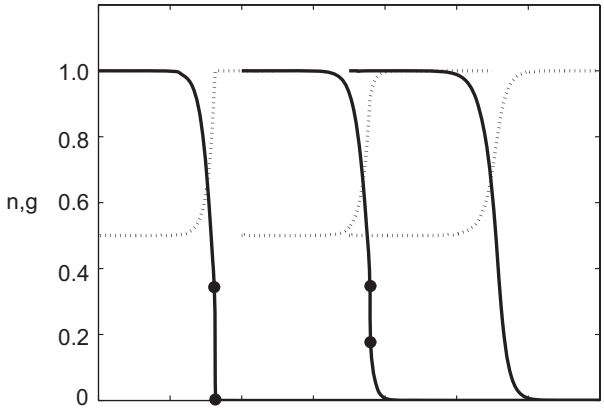

FIG. 6.5. *Numerical profiles for $n(x,t)$ (solid line) and $g(x,t)$ (dotted line) with $\gamma = 1.0$, $\beta = 1.0$. Left to right $n(x,t)$: Discontinuous solution with maximum shock length ($n_R = 0$) with $\xi_1 = 3.0$; discontinuous solution with smaller shock length ($n_R > 0$) with $\xi_1 = 1.5$; continuous solution with $\xi_1 = 1$. The end points of the shocks (•) are shown. Numerical computations were performed with $\Delta x = 0.05$ and $\Delta t = 0.01$.*

wall to the completely colonized steady state, as in Figure 6.4(b). The middle profile in Figure 6.5 corresponds to an initial condition where the decay is moderate. This profile shows a smaller discontinuity in the cell density; however, the discontinuity does not extend to the base of the profile as the toe of the profile is continuous. Again there is a discontinuity in the gradient of the chemoattractant at the same position where the discontinuity in the cell density occurs. Finally, with a slowly decaying initial condition, the distributions of the cell density, chemoattractant concentration, and the gradient of the chemoattractant concentration are continuous, as shown in the rightmost profile. The phase plane corresponding to this final case has the two steady states on the same side of the wall, as in Figure 6.4(a). With the parameter values used in Figure 6.3, the numerical solutions are qualitatively similar.

The profiles in Figure 6.5, together with the phase diagrams in Figures 6.3 and 6.4, give a comprehensive understanding of the behavior of the traveling wave solutions obtained from (2.7)–(2.8) when $D = 0$ and chemotaxis is the only cell migration process. Similar to the alternative diffusion-only case ($\chi = 0$), the existence of traveling wave solutions is established. In contrast, migration by pure diffusion cannot give rise to discontinuous solutions because of the smoothing nature of linear diffusion. However, both these limiting cases show that the speed of the resulting traveling wave solution is determined by the exponential decay rate of the initial distribution of the migrating cell population.

Finally, it follows from our scaling arguments (2.6), (6.3)–(6.4), that the minimum wave speed for the chemotaxis-only migration case scales with $\sqrt{\chi}$ and hence has the form

$$c_{min} = K(\beta,\gamma)\sqrt{\chi}, \tag{6.10}$$

where $K(\beta,\gamma)$ is a constant dependent on the kinetic parameters. This was anticipated in the earlier numerical simulations presented in Figure 4.1(a). Therefore c_{min} has a similar form to the minimum wave speed of $2\sqrt{D}$ for the diffusion driven migration as discussed in section 6.1. The major difference is that the coefficient $K(\beta,\gamma)$ is

not a constant but varies in a complicated way with the kinetic parameters β and γ. The two examples discussed above provide the criterion for determining K. As in Example 1, if $c_{min}^2 > \frac{\beta\gamma}{\beta+\gamma}$, then c_{min} is defined as that value of c such that the trajectory from the hole in the wall passes through $(1, c^2/\gamma)$. Alternatively, as in Example 2, if $c_{min}^2 < \frac{\beta\gamma}{\beta+\gamma}$, then c_{min} is defined as that value of c such that the trajectory from the steady state $(\frac{\beta}{\beta+\gamma}, 1)$ passes through $(1, c^2/\gamma)$.

An analytical solution for $K(\beta, \gamma)$ has been attempted but does not appear possible at the present time. Instead, numerical solutions are used to compute the minimum wave speed $K(\beta, \gamma)$ over a range of kinetic parameters β and γ. The form of $K(\beta, \gamma)$ is shown in Figure 6.6. In general, $K(\beta, \gamma)$ decreases with increasing β and increases with increasing γ, that is, $\frac{\partial K}{\partial \beta} < 0$ and $\frac{\partial K}{\partial \gamma} > 0$. These trends can be understood by considering the biological processes associated with the kinetic terms. The steady state concentration $g = \frac{\beta}{\gamma+\beta}$ increases with increasing β or with decreasing γ. As this steady concentration increases, the chemotactic gradient decreases giving rise to slower traveling wave speeds and a reduced value of $K(\beta, \gamma)$. This intuitive argument agrees with the form of $K(\beta, \gamma)$ deduced with the numerical solutions shown in Figure 6.6. We also investigated whether $K(\beta, \gamma)$ depended on a similarity variable, such as the ratio $\frac{\beta}{\gamma}$ alone, as illustrated in Figure 6.6(c). It appears that $K(\beta, \gamma)$ has a similar shape for the wide range of $\frac{\beta}{\gamma}$ investigated. However, the location of the curve can vary considerably for various choices of β.

Incorporating both numerical and phase plane analyses in this work reveals a remarkable advantage regarding the development and testing of the numerical algorithm. In general, testing numerical schemes for coupled nonlinear migration problems can be very difficult because of a lack of suitable analytical solutions [35]. Using the phase plane for the pure chemotaxis problem quantifies certain properties of the solution, such as the critical wave speed c_{crit}, the minimum wave speed c_{min}, and the size of the discontinuity. This unique information is useful in developing the numerical scheme as these quantitative checks are invoked to ensure that the numerical scheme is accurate.

6.3. Migration with both diffusion and chemotaxis. A three-dimensional phase plane analysis of (5.1)–(5.3) does not provide a productive way for seeking traveling wave solutions. A numerical study is convenient for examining both the shape of the invading profile as well as the minimum wave speeds. In particular, the robust numerical algorithm presented here has no difficulty in generating numerical solutions for any value of the diffusion coefficient and chemotactic factor. Therefore, it is of interest to investigate how this general case of combined chemotaxis and diffusive migration relates to the two limiting cases when either D or χ is zero.

6.3.1. Numerical solution profiles. Various solution profiles showing the influence of increasing the chemotactic factor χ for a fixed value of diffusivity $D = 1$ are shown in Figure 6.7(a). Comparison of these profiles shows that their smooth shape evolves to one with a developing discontinuity as χ increases. Moreover, the gradient of both the cell density and chemoattractant concentration increases with χ. Since the profiles are plotted at a fixed time starting from the same initial data, the wave speed clearly increases with χ from the minimum wave speed associated with the Fisher equation. This increase in wave speed with χ is expected because the inclusion of a second migration process enhances cell migration.

Similarly, the effect of increasing D on the numerical solutions is shown in Figure 6.7(b). Now the steep profiles evolve to smooth, flatter profiles as the diffusivity

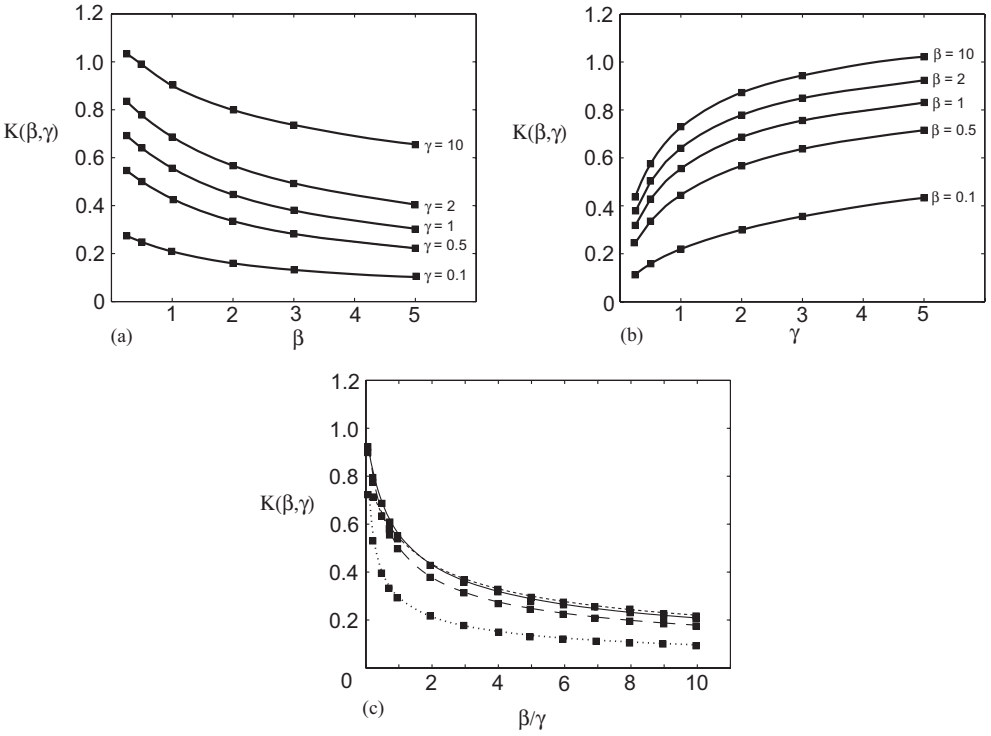

FIG. 6.6. *Dependence of $K(\beta,\gamma)$ on the kinetic parameters.* (*a*) *β for various γ values;* (*b*) *γ for various β values;* (*c*) *β/γ for $\beta = 10$ (short dashed line), $\beta = 1$ (solid line), $\beta = 0.5$ (long dashed line), and $\beta = 0.1$ (dotted line).*

increases, which reflect the smoothing nature of linear diffusion. These flatter profiles travel at a faster rate, as for the Fisher equation [25].

It is interesting to compare the rate at which the added migration processes competes with the underlying migration. In Figure 6.7(a), with the addition of chemotaxis to diffusive migration, the shape of the front steepens with increasing χ; however, the smooth shape is maintained fairly consistently up until $\chi = 50$ and it is not until $\chi = 100$ that the profile begins to tend toward the upper limit of chemotaxis-only migration with a discontinuous front. Conversely, in Figure 6.7(b), with the addition of diffusion to chemotactic migration, the shape of the front is very sensitive to the addition of a small amount of diffusion. The sharp front is smoothed with increasing D and tends toward the limit of diffusion-only migration for $D = 0.5$. These observations show that diffusion masks the influence of chemotaxis more efficiently than chemotaxis masks diffusion. These trends will now be more thoroughly explored in terms of the minimum wave speed c_{min}.

6.3.2. Minimum wave speed. For the system (5.1)–(5.3), a linear stability analysis of the steady state $(g, n, v) = (1, 0, 0)$ gives real eigenvalues if and only if $c \geq 2\sqrt{D}$, ensuring the point is a saddle point, just like for the Fisher equation. This condition provides a lower bound for the minimum wave speed. Numerical computations provide an extended analysis of the influence of mixed migration on the minimum wave speed. We examine the case where one of χ or D is held constant while simultaneously varying the other migration parameter. Numerical computations are

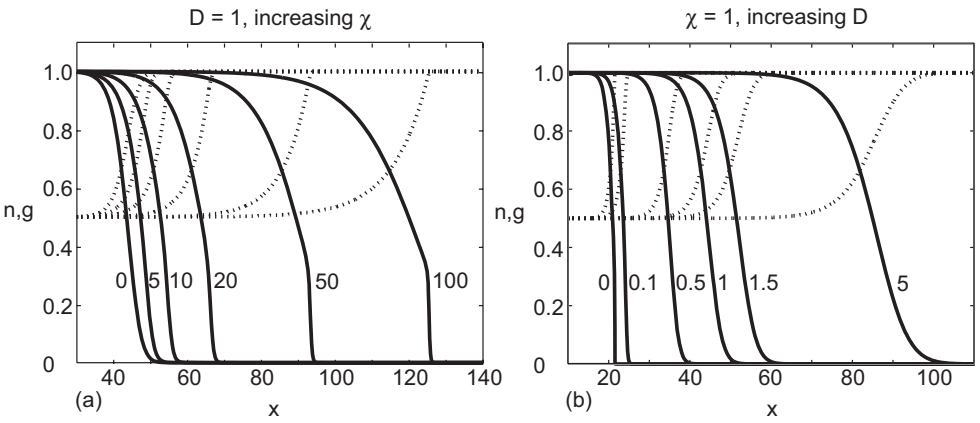

FIG. 6.7. *Numerical profiles of* $n(x, 20)$ (*solid line*) *and* $g(x, 20)$ (*dotted line*). (*a*) *The influence of increasing chemotaxis with fixed* $D = 1$, *with* χ *increasing from left to right with values indicated.* (*b*) *The influence of increasing diffusion with fixed* $\chi = 1$, *with* D *increasing from left to right with values indicated. All results were computed with* $\beta = 1, \gamma = 1$, $\xi_1 = 10$, $\Delta x = 0.05$, *and* Δt *was varied depending on* χ.

conducted to determine the effect on c_{min}.

Fixing the value of the chemotactic factor, namely, $\chi = 1$, the minimum wave speed increases monotonically with the diffusion coefficient D, as shown in Figure 6.8(a). Furthermore, as the diffusion coefficient increases, the minimum wave speed asymptotes to $2\sqrt{D}$. For this choice of kinetic parameters, $2\sqrt{D}$ provides a good approximation to c_{min} when $D/\chi > 0.2$. In general, for sufficiently large D/χ, diffusion dominates over chemotaxis and the minimum wave speed is accurately approximated by the Fisher wave speed $c_{min} = 2\sqrt{D}$, while for smaller values of D/χ, chemotaxis dominates and c_{min} is greater than that associated with the Fisher equation or chemotaxis alone. The numerical results for large D lie a little below $2\sqrt{D}$; this trend was also found for haptotactic invasion with added diffusion [19].

Similarly, setting the diffusion coefficient as $D = 1$, the c_{min} monotonically increases with the chemotactic factor χ and asymptotes to $K(\beta, \gamma)\sqrt{\chi}$, as illustrated in Figure 6.8(b). In this example, $K(\beta, \gamma)\sqrt{\chi}$ gives a good approximation to c_{min} when $\chi/D > 50.0$. In general for sufficiently large χ/D, chemotaxis dominates over diffusion and the minimum wave speed is well approximated by $c_{min} = K(\beta, \gamma)\sqrt{\chi}$ as given in (6.10). Conversely, for smaller values of χ/D, diffusion dominates and c_{min} is greater than that associated with chemotaxis or diffusion alone.

An explicit formula for c_{min} as a function of χ and D (as well as the kinetic parameters) has not been determined at this stage. However, some descriptive comments can be made. The discussion above indicates a natural lower bound for c_{min} as $\max[K(\beta, \gamma)\sqrt{\chi}, 2\sqrt{D}]$. An upper bound can be conjectured, as indicated in Figure 6.8. These can be combined as

$$\max[K(\beta, \gamma)\sqrt{\chi}, 2\sqrt{D}] < c_{min} < \sqrt{4D + K^2(\beta, \gamma)\chi}. \tag{6.11}$$

This expression suggests that diffusion dominates over chemotaxis when $\frac{K^2(\beta,\gamma)\chi}{4D} \ll 1$, and alternatively that chemotaxis dominates over diffusion when $\frac{4D}{K^2(\beta,\gamma)\chi} \ll 1$.

6.3.3. Perturbation analysis. When chemotaxis is small compared to diffusive migration, namely, $\chi/D \ll 1$, a regular perturbation analysis could be undertaken to

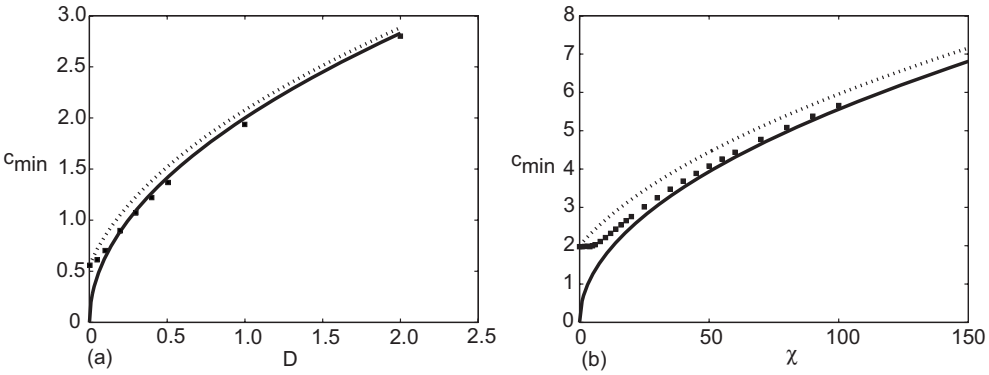

FIG. 6.8. *Numerically calculated minimum wave speed c_{min} shown with squares evolving from initial data with $\xi_1 = 10$. Results computed with $\beta = 1, \gamma = 1$. (a) Dependence on D with $\chi = 1$. The solid curve is $c_{min} = 2\sqrt{D}$. (b) Dependence on χ with $D = 1$. The solid curve is $c_{min} = K(\beta,\gamma)\sqrt{\chi}$; for this example $K(\beta,\gamma) \approx 0.556$. The dotted curves are the conjectured upper bound $c_{min} = \sqrt{4D + K^2(\beta,\gamma)\chi}$.*

give a solution valid for small χ/D. The first-order terms for n would just be the solution to the Fisher equation. This analysis is not very insightful and therefore is not shown here. A more illuminating analysis comes from the alternative case when D/χ is small.

Marchant [19] examined the case where a small amount of diffusion was added to a haptotactic invasion problem, using singular perturbation and phase plane arguments. A similar analysis is performed here but can be taken further and solved exactly. As discussed in section 6.2, when $D = 0$, our model supports discontinuous traveling wave solutions for a range of values of c. We know that a small amount of diffusion added to a purely chemotactic system has the effect of smoothing out any discontinuities. However, the gradients are expected to remain large in a small region. When D/χ is small, a perturbation analysis provides an understanding of the transition region. The analysis determines the evolution from a discontinuous traveling wave solution ($D = 0$) to one which is smooth, but has large derivative, in a small critical layer. Set $\chi = 1$ without any loss of generality. With $D \ll 1$, we seek solutions to (5.1)–(5.3) as an asymptotic expansion in terms of D as

$$g = g_0(z) + Dg_1(z) + D^2 g_2(z) + \cdots, \tag{6.12}$$

$$n = n_0(z) + Dn_1(z) + D^2 n_2(z) + \cdots, \tag{6.13}$$

$$v = v_0(z) + Dv_1(z) + D^2 v_2(z) + \cdots. \tag{6.14}$$

Hence g_0 and n_0 will satisfy (6.3)–(6.4). We choose to consider the traveling wave solution with the minimum wave speed c_{min}. We shift the origin so that the jump occurs at $z = 0$. This solution is the first term in the *outer* solution of the asymptotic expansion of the solution. At $z = 0$, for small D, there will be a narrow region where the rates of change of n are large, since n has to connect the left-hand limit n_L and right-hand limit $n_R = 0$. In this critical layer we seek a solution in the expanded variable $\xi = z/D$ as

$$g = G_0(\xi) + DG_1(\xi) + D^2 G_2(\xi) + \cdots, \tag{6.15}$$

$$n = N_0(\xi) + DN_1(\xi) + D^2 N_2(\xi) + \cdots, \tag{6.16}$$

$$v = \frac{1}{D}V_0(\xi) + V_1(\xi) + DV_2(\xi) + \cdots. \tag{6.17}$$

Substitution into (5.1)–(5.3) yields the highest-order terms satisfying

$$\frac{dG_0}{d\xi} = 0, \tag{6.18}$$

$$\frac{dN_0}{d\xi} = V_0, \tag{6.19}$$

$$\frac{dV_0}{d\xi} = -\left[1 + \frac{1}{c_{min}^2}(\beta(1-G_0) - 2\gamma N_0 G_0)\right] c_{min} V_0. \tag{6.20}$$

For the inner solution to match the outer solution, we require

$$G_0 = 1, \quad \xi \to \pm\infty, \tag{6.21}$$

$$N_0 = n_L = \frac{c_{min}^2}{\gamma}, \quad \xi \to -\infty\,, \qquad N_0 = n_R = 0, \quad \xi \to \infty, \tag{6.22}$$

$$V_0 = 0, \quad \xi \to \pm\infty. \tag{6.23}$$

Note that the value of n_L is obtained using the jump condition (6.7). Equations (6.18) and (6.21) give $G_0(\xi) = 1$ for all ξ. This simplifies the coupled system (6.19)–(6.20) as

$$\frac{dV_0}{d\xi} = -\left[1 - \frac{2\gamma}{c_{min}^2}N_0\right] c_{min}\frac{dN_0}{d\xi} = -c_{min}\left[\frac{dN_0}{d\xi} - \frac{2\gamma}{c_{min}^2}N_0\frac{dN_0}{d\xi}\right], \tag{6.24}$$

which integrates to

$$\frac{dN_0}{d\xi} = V_0 = -c_{min}\left(N_0 - \frac{\gamma}{c_{min}^2}N_0^2\right), \tag{6.25}$$

where the integration constant is zero from the conditions at $\xi \to \infty$. This is a logistic equation with solution

$$N_0 = \frac{c_{min}^2}{\gamma}\frac{e^{-c_{min}\xi}}{1 + e^{-c_{min}\xi}}, \tag{6.26}$$

where $N_0(0) = c_{min}^2/(2\gamma)$ with no loss of generality. Therefore, adding a small amount of diffusion introduces a steep transition region, of width D with exponential behavior depending on $c_{min}z/D$ (having set $\chi = 1$).

Figure 6.9 compares the numerically generated solutions to the perturbation analysis logistic solution (6.26). The region about the sharp front is stretched via the transformation $\xi = z/D$ so that the gradient is $\mathcal{O}(1)$ in the ξ coordinate. The numerical profile is translated so that $n(\xi, t) = c_{min}^2/(2\gamma)$ occurs at $\xi = 0$, as it does for N_0. The profiles of the leading order perturbation analysis and the numerically generated solution compare very well in the leading edge for $\xi > 0$ for small values of D as shown. The perturbation solution does not match as well in the region $\xi < 0$ for two reasons. First, we have matched with the jump density n_L as $\xi \to -\infty$, whereas the full numerical solution goes to the $n = 1$ state. Second, the slope of n as $\xi \to -\infty$ does not match at this dominant order of the approximation. The next order term, V_1, would be required to match the slope of the outer solution $\frac{\partial n_0}{\partial z}$ at the left of the shock as $\xi \to -\infty$.

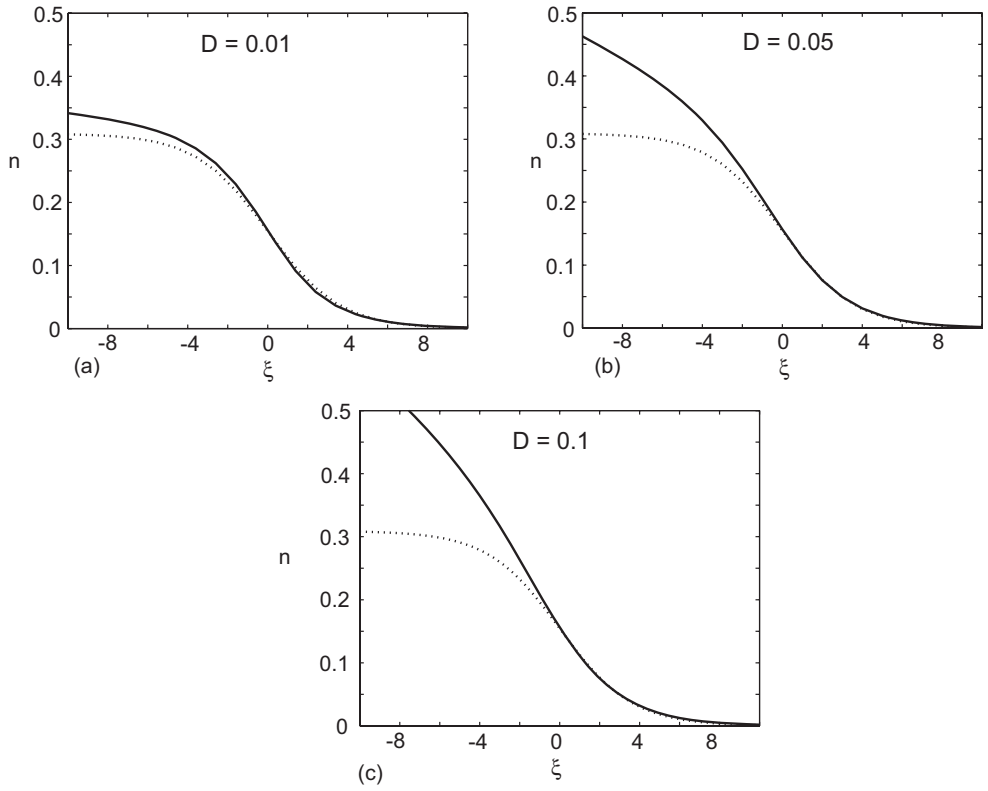

FIG. 6.9. *Critical layer comparison of numerical solution with the dominant perturbation solution* $N_0(\xi)$ *in* (6.26). *The solid curve is the numerical solution* $n(\xi, 20)$ *and the dotted curve is* $N_0(\xi)$. *Results computed with* $\chi = 1$, $\beta = 1, \gamma = 1$ *and using initial data with* $\xi_1 = 10$. (*a*) $D = 0.01$, (*b*) $D = 0.05$, (*c*) $D = 0.1$.

7. Conclusions. This article considers a mathematical model of cell invasion, where both diffusion and chemotaxis are the migration mechanisms. The details of the model were developed such that the results of the analysis are applicable to certain cell migration processes which are known to occur in developmental biology. A suite of traveling wave solutions is shown to exist regardless of whether the migration is pure diffusive, pure chemotaxis, or a combination of diffusive and chemotaxis migration. For all three cases, the traveling wave speed is bounded from below. The minimum wave speed is always observed whenever numerical simulations are performed using initial data where the cell density has compact support. Since the initial distribution of invading cells usually falls to zero for x large enough, this seems to be the most biologically relevant situation. Therefore, in general the most biologically relevant solution for these cell migration models is the solution corresponding to the minimum wave speed.

An understanding of the nature of the minimum wave speed as a function of the migration parameters is important. Phase plane analysis can provide values for the minimum wave speed for the two limiting cases when either the migration is purely diffusive or chemotactic. These values and the explicit shapes of the solutions can also be found using numerical methods. In particular, a robust numerical algorithm is developed which gives stable traveling waves solutions including shocks. The numeri-

cal algorithm combines a high-accuracy explicit central scheme [14] for the nonlinear hyperbolic and reaction terms together with a standard implicit finite element solution of the diffusion term with an operator split approach. The use of operator splitting for this particular problem was critical in combining the numerical solutions of the chemotaxis and diffusion terms together in a way that conveniently minimized numerical stability issues. Therefore, the numerical algorithm presented in this work provides an extremely accurate and versatile means of solving combined chemotaxis and diffusive migration problems.

For the combined diffusion and chemotactic migration case, numerical results were used to determine an upper and a lower bound on the minimum wave speed. Numerical results also demonstrate how the diffusion and chemotaxis mechanisms interact in a combined migration problem. The rate at which the minimum wave speed for the mixed migration case approached the minimum wave speed for the two limiting cases indicated that diffusion dominates over chemotaxis for relatively small values of the ratio of $\frac{D^*}{\chi^*} = \frac{D\lambda_3}{\chi\lambda_2}$.

The results from the combined diffusion and chemotaxis case indicate that adding a small amount of diffusion to a pure chemotaxis problem can result in the chemotactic characteristics of the problem being completely masked by the added diffusion. This observation is particularly relevant for numerical computations, when parabolic solvers are often used for chemotaxis (or haptotaxis) dominated processes. Further, this result also implies that standard numerical solutions of chemotaxis problems might be extremely sensitive to numerical diffusion and so great care should be exercised in obtaining such solutions.

In summary, this analysis provides a deeper qualitative and quantitative understanding of the interplay between diffusion and chemotaxis for invading cell populations. Often, when modeling biological cell migration, parameter values are difficult to estimate. If the wave speed can be determined experimentally, and the diffusion rate estimated, then some reasonable estimates of the chemotactic term may be deduced from the results presented here.

REFERENCES

[1] H. M. Byrne, M. A. J. Chaplain, G. J. Pettet, and D. L. S. McElwain, *A mathematical model of trophoblast invasion,* J. Theoret. Med., 1 (1999), pp. 275–286.

[2] H. M. Byrne, M. A. J. Chaplain, G. J. Pettet, and D. L. S. McElwain, *An analysis of a mathematical model of trophoblast invasion*, Appl. Math. Lett., 14 (2001), pp. 1005–1010.

[3] R. Courant and D. Hilbert, *Methods of mathematical physics. Vol.* II, 2nd ed., Interscience, New York, 1964.

[4] J.Crank, *The Mathematics of Diffusion*, 2nd ed., Oxford University Press, Oxford, UK, 1975.

[5] D. Dormann and C. J. Weijer, *Chemotactic cell movement during development*, Curr. Opin. Genet. Dev., 13 (2003), pp. 358–364.

[6] R. A. Fisher, *The wave of advance of advantageous genes*, Ann. Eugenics, 7 (1937), pp. 353–369.

[7] R. M. Ford and P. T. Cummings, *Mathematical models of bacterial chemotaxis,* in Mathematical Modeling in Microbial Ecology, A. L. Koch, J. A. Robinson, and G. A. Milliken, eds., Chapman and Hall, New York, 1998, pp. 228–269.

[8] R. M. Ford and D. A. Lauffenburger, *Analysis of chemotactic bacterial distributions in population migration assays using a mathematical model applicable to steep or shallow attractant gradients,* Bull. Math. Biol., 53 (1991), pp. 721–749.

[9] C. J. Hearn, M. Murphy, and D. F. Newgreen, *GDNF and ET-3 differentially modulate the numbers of avian enteric neural crest cells and enteric neurons in vitro,* Dev. Biol., 197 (1998), pp. 93–105.

[10] T. Hillen, *Hyperbolic models for chemosensitive movement,* Math. Models Methods Appl. Sci., 12 (2002), pp. 1007–1034.

[11] D. Horstmann and A. Stevens, *A constructive approach to traveling waves in chemotaxis,* J. Nonlinear Sci., 14, (2004), pp. 1–25.
[12] J. Kassis, D. A. Lauffenburger, T. Turner, and A. Wells, *Tumor invasion as dysregulated cell motility,* Sem. Cancer. Biol., 11 (2001), pp. 105–119.
[13] E. F. Keller and L. A. Segel, *Travelling bands of chemotactic bacteria: A theoretical analysis,* J. Theoret. Biol., 30 (1971), pp. 235–248.
[14] A. Kurganov and E. Tadmor, *New high-resolution central schemes for non-linear conservation laws,* J. Comput. Phys., 160 (2000), pp. 241–282.
[15] N. M. Le Douarin and M. A. M. Teillet, *Experimental analysis of the migration and differentiation of the autonomic nervous system and of neurectodermal mesenchymal derivatives using a biological cell marking technique,* Dev. Biol., 41 (1974), pp. 162–184.
[16] R. J. LeVeque and J. Oliger, *Numerical methods based on additive splittings for hyperbolic partial differential equations,* Math. Comput., 40 (1983), pp. 469–497.
[17] K. A. Landman, G. J. Pettet, and D. F. Newgreen, *Mathematical models of cell colonisation of uniformly growing domains,* Bull. Math. Biol., 65 (2003), pp. 235–262.
[18] K. A. Landman, G. J. Pettet, and D. F. Newgreen, *Chemotactic cellular migration: Smooth and discontinuous travelling wave solutions,* SIAM J. Appl. Math., 63 (2003), pp. 1666–1681.
[19] B. P. Marchant, *Modelling Cell Invasion*, Ph.D. thesis, University of Oxford, Oxford, UK, 1999.
[20] B. P. Marchant, J. Norbury, and A. J. Perumpanani, *Travelling shock waves arising in a model of malignant invasion,* SIAM J. Appl. Math., 60 (2000), pp. 463–476.
[21] B. P. Marchant, J. Norbury, and J. A. Sherratt, *Travelling wave solutions to a haptotaxis-dominated model of malignant invasion,* Nonlinearity, 14 (2001), pp. 1653–1671.
[22] B. P. Marchant and J. Norbury, *Discontinuous travelling wave solutions for certain hyperbolic systems,* IMA J. Appl. Math., 67 (2002), pp. 201–224.
[23] H. P. McKean, *Application of Brownian motion to the equation of Kolmogorov-Petrovskii-Piskunov,* Comm. Pure Appl. Math., 28 (1975) pp. 323–331.
[24] J. D. Murray and M. R. Myerscough, *Pigmentation pattern formation on snakes,* J. Theoret. Biol., 149 (1991), pp. 339–360.
[25] J. D. Murray, *Mathematical Biology,* 2nd ed., Springer-Verlag, Heidelberg, 1993.
[26] D. Natarajan, C. Marcos-Gutierrez, V. Pachnis, and E. de Graaff, *Requirement of signalling by receptor tyrosine kinase RET for the directed migration of enteric nervous system progenitor cells during mammalian embryogenesis,* Development, 129 (2002), pp. 5151–5160.
[27] D. F. Newgreen, *Control of the directional migration of mesenchyme cells and neurites,* Sem. Developmental Biol., 1 (1990), pp. 301–311.
[28] D. F. Newgreen, B. Southwell, L. Hartly, and I. J. Allan, *Migration of enteric neural crest cells in relation to growth of the gut in avian embryos,* Acta Anat., 157 (1996), pp. 105–115.
[29] H. G. Othmer and A. Stevens, *Aggregation, blowup, and collapse: The ABC's of taxis in reinforced random walks,* SIAM J. Appl. Math., 57 (1997), pp. 1044–1081.
[30] A. J. Perumpanani, J. A. Sherratt, J. Norbury, and H. M. Byrne, *A two parameter family of travelling waves with a singular barrier arising from the modelling of extracellular matrix mediated cell invasion,* Phys. D, 126 (1999), pp. 145–159.
[31] G. J. Pettet, H. M. Byrne, D. L. S. McElwain, and J. Norbury, *A model of wound-healing angiogenesis in soft tissue,* Math. Biosci., 136 (1996), pp. 35–63.
[32] G. J. Pettet, D. L. S. McElwain, and J. Norbury, *Lotka–Volterra equations with chemotaxis: Walls, barriers and travelling waves,* IMA J. Math. Appl. Med. Biol., 17 (2000), pp. 395–413.
[33] W. H. Press, B. P. Flannery, S. A. Teukolsky, and W. T. Vetterling, *Numerical Recipes in FORTRAN: The Art of Scientific Computing,* 2nd ed., Cambridge University Press, Cambridge, UK, 1992.
[34] L. J. Segerlind, *Applied Finite Element Analysis,* 2nd ed., John Wiley and Sons, Singapore, 1984.
[35] M. J. Simpson and T. P. Clement, *A theoretical analysis of the worthiness of Henry and Elder problems as benchmarks of density-dependent groundwater flow models,* Adv. Water Resour., 26 (2003), pp. 17–31.
[36] M. J. Simpson, K. A. Landman, and T. P. Clement, *Assessment of a non-traditional operator split algorithm for simulation of reactive transport*, Math. Comput. Simulation, in press, 2005.

[37] M. Starz-Gaiano and D. J. Montell, *Genes that drive invasion and migration in Drosophila,* Curr. Opin. Genet. Dev., 14 (2004), pp. 86–91.

[38] G. Strang, *On the construction and comparison of difference schemes,* SIAM J. Numer. Anal., 5 (1968), pp. 506–517.

[39] R. T. Tranquillo, *Perspectives and models of gradient perception,* in Biology of the Chemotactic Response, J. P. Armitage and J. M. Lackie, eds., Cambridge University Press, Cambridge, UK, 1991, pp. 35–75.

[40] R. T. Tranquillo and W. Alt, *Receptor-mediated models for leukocyte chemotaxis,* in Dynamics of Cell and Tissue Motion, W. Alt, A. Deutsch, and G. Dunn, eds., Birkhäuser, Berlin, 1997, pp. 141–147.

[41] A. J. Valocchi and M. Malmstead, *Accuracy of operator splitting for advection-dispersion-reaction problems,* Water Resour. Res., 28 (1992), pp. 1471–1476.

[42] G. T. Yeh, *Computational Subsurface Hydrology. Reactions, Transport and Fate,* Kluwer Academic Publishers, Norwell, MA, 2000.

[43] H. M. Young, C. J. Hearn, P. G. Farlie, A. J. Canty, P. Q. Thomas, and D. F. Newgreen, *GDNF is a chemoattractant for enteric neural crest cells,* Dev. Biol., 229 (2001), pp. 503–516.

[44] C. Zheng and G. D. Bennett, *Applied Contaminant Transport Modelling,* John Wiley and Sons, New York, 2002.